ChemCatChem

Research Article
doi.org/10.1002/cctc.202200059

Chemistry Europe
European Chemical Societies Publishing

www.chemcatchem.org

Consequences of Intrapore Liquids on Reactivity, Selectivity, and Stability for Aldol Condensation Reactions on Anatase TiO_2 Catalysts

Shashikant A. Kadam,[a, b] Andrew Hwang,[a] and Enrique Iglesia*[a]

This study provides evidence and mechanistic interpretations for the significant consequences of intrapore non-polar liquids on acetone aldol condensation turnover rates, selectivity to primary dimer products, and catalyst stability for reactions at Lewis acid-base site pairs on TiO_2 surfaces. These non-polar liquids confer such benefits through the preferential stabilization of transition states (TS) for adsorption ("entry") and desorption ("exit") steps, which place their respective reactants or products within a solvating outer sphere environment. The extent to which non-polar fluids (*n*-heptane) form an intrapore liquid phase within TiO_2 voids was obtained from N_2 uptakes using established formalisms that consider the different molal volume, surface tension, and volatility between N_2 and *n*-heptane. Acetone condensation rates are limited by C–H activation, an "entry" step that forms bound prop-1-en-2-olates via a TS stabilized by intrapore liquids, leading to higher aldol condensation turnover rates as *n*-heptane pressure increases and active TiO_2 surfaces become increasingly immersed within a non-polar liquid phase. These liquids solvate the late TS structures that mediate the desorption of primary C_6 condensation products even more effectively than those involved in prop-1-en-2-olate formation or in nucleophilic attack events that later form C–C bonds. Such preferential solvation favors desorption over C–C coupling events, thus disfavoring the formation of larger oligomers that become stranded at active sites, thus leading to much slower deactivation. Moreover, solvation by non-polar liquids also leads to C_6 alkanones as the sole products formed in a single surface sojourn. These effects of a non-polar dense phase circumvent the inherent stability, reactivity, and selectivity hurdles that have precluded practical aldol condensation catalysis on Lewis acid-base pairs at oxide surfaces; these consequences are demonstrated here for TiO_2 catalysts, acetone aldol condensation reactions, and *n*-heptane as the non-polar liquid but through strategies, concepts, and mechanistic features that extend to other systems. More generally, these observations and their mechanistic origins demonstrate how a contacting liquid preferentially solvates TS structures for elementary steps that involve either reactants arriving from or products entering into an outer sphere environment that contains a dense non-polar phase.

Introduction

Aldol condensation reactions convert carbonyl compounds (and related oxygenates) into products of higher value by removing O-atoms and forming new C–C bonds, thus leading to less volatile products with higher energy densities.[1–8] Such reactions are catalyzed by Lewis acid-base site pairs on TiO_2 and ZrO_2; an exposed cation (Ti^{4+} or Zr^{4+}) acts in concert with a vicinal oxygen anion to mediate the bond cleavage and formation steps involved in aldol condensation turnovers.[9,14,27] These reactions form α,β-unsaturated alkanals and alkanones via steps that include the kinetically-relevant cleavage of the α-C–H bonds in reactants and subsequent nucleophilic attack of carbonyls by enolates and dehydration of the resulting aldol species;[9–17] these mechanistic routes resemble those that mediate C–C bond formation and O-removal in reactions of carboxylic acids (ketonization).[9,17–25] The unsaturated primary products formed in aldol condensation events can react further to form larger molecules, which bind strongly onto Ti–O and Zr–O acid-base pairs, leading to selectivity losses and fast deactivation.[12,14–15,26–28]

The steps that form the primary unsaturated oxygenates can reach near-equilibrium conversions on competent catalysts,[11] but the significant bed residence times required to achieve such conversions also favor sequential chain growth.[10,12] The resulting deactivation and loss of primary products not only interfere with rigorous kinetic inquiries[14,27] required for unequivocal mechanistic conclusions, but also preclude the efficient use of these reactions in practice. Several recent studies have reached contradictory conclusions about the identity of the kinetically-relevant steps and the most abundant bound intermediates in surface-catalyzed aldol condensation reactions. Acetaldehyde condensation was proposed to occur via kinetically-relevant reactant adsorption or product desorption steps on TiO_2 surfaces that had become densely-covered by organic residues, thus predominantly exposing residual Ti–O centers that become isolated within such

[a] S. A. Kadam, A. Hwang, Prof. E. Iglesia
Department of Chemical and Biomolecular Engineering
University of California
Berkeley, CA 94720 (USA)
E-mail: iglesia@berkeley.edu
[b] S. A. Kadam
Department of Nanocatalysis
J. Heyrovský Institute of Physical Chemistry
The Czech Academy of Sciences
182 00, Prague (Czech Republic)

Supporting information for this article is available on the WWW under https://doi.org/10.1002/cctc.202200059

adlayers;[15] other studies, also conducted on catalysts after their significant deactivation, proposed that rates are limited instead by nucleophilic attack on bound acetaldehyde by bound enolates.[16] In both instances, the evidence was based on kinetic trends observed on surfaces decorated by significant coverages of unreactive species.

Mechanistic studies based on kinetic analysis were combined with spectroscopic, isotopic, and theoretical methods on TiO_2 surfaces protected from deactivation by scavenging unsaturated primary products through hydrogenation by H_2 on a co-mixed Cu-based catalytic function.[14,27] These studies showed that enolate formation at Ti–O acid-base site pairs on essentially bare surfaces is the sole kinetically-relevant step for a broad range of alkanal and alkanone reactants.[14,27] The transition states that mediate such steps involve concerted interactions with acid-base site pairs, in which O-atoms abstract the H-atom located at the α-position to the carbonyl group and Ti centers stabilize enolate moieties as they incipiently form. TiO_2 surfaces densely-covered by unreactive residues lead to Ti–O pairs that become isolated, thus disfavoring the bimolecular steps that form C–C bonds, but which require accessible vicinal Ti–O pairs. As a result, the kinetic relevance shifts from monomolecular enolate formation at a single Ti–O pair on protected clean surfaces[14,27] to bimolecular C–C bond formation steps at vicinal pairs[16] as unreactive organic residues form on unprotected TiO_2 surfaces.

This study reports an alternate strategy to inhibit secondary reactions and concomitant deactivation events without requiring another function or the presence of H_2, thus leading to unsaturated primary products with high selectivity. Stability and selectivity improvements are achieved through the purposeful capillary condensation of a non-polar inert intrapore liquid phase. This liquid phase strongly influences reactivity, selectivity, and catalyst stability for monofunctional anatase TiO_2 surfaces by preferentially stabilizing specific transition states that mediate kinetically-relevant and selectivity-determining steps. These findings parallel the recent demonstration of enhanced stability and primary dimer selectivities upon formation of an intrapore non-polar liquid phase for ethene, propene, and butene dimerization reactions on Ni-MCM-41 catalysts.[29,30] As in the case of acetone condensation in the present study, alkene dimerization involves C–C bond formation to give dimers that can undergo subsequent C–C bond formation events, leading to larger oligomers that ultimately block active sites. Alkene dimerization turnovers are limited by C–C bond formation steps via transition states that are predominantly stabilized by binding onto active sites, leading to turnover rates that are affected only weakly by the presence of intrapore liquids.[29,30]

Aldol condensation rates on TiO_2 are limited by C–H bond dissociation in carbonyl reactants to form enolates; such steps involve transition states that retain some reactant character and are therefore stabilized by a contacting liquid phase. As a result, acetone condensation rates can benefit from the presence of a non-polar liquid phase. Indeed, the intrapore condensation of *n*-heptane increased turnover rates, selectivity, and stability for acetone condensation reactions on mesoporous anatase TiO_2 catalysts. These findings and their mechanistic interpretation provide evidence for how transition states sense their solvation by liquids and how these "outer sphere" effects depend on the extent to which these transition states are stabilized by direct coordination to binding points (inner sphere) or through interactions with a liquid environment (outer sphere); the latter interactions become most consequential when entry (adsorption) or exit (desorption) steps limit rates, because their respective early and late transition states place such species, at least in part, within the surrounding liquid environment.[31,32] These concepts and their catalytic consequences are illustrated here for acetone reactants, using *n*-heptane as the non-polar liquid, and for anatase TiO_2 as the catalyst; the concepts and the mechanistic framework, however, are broadly applicable and general. To our knowledge, no previous strategies have prevented the fast deactivation of TiO_2-based monofunctional catalysts, even though the competence (and impractical selectivities and deactivation rates) of such catalysts was first demonstrated nearly four decades ago.[10,12]

Results and Discussion

Reactions and elementary steps for acetone condensation on anatase

Reactions of acetone (0.5–2.5 kPa; 363 K) on anatase TiO_2 (TiO_2(a)) form C_6 and C_9 alkanones as detectable products. Mesityl oxide (4-methylpent-3-en-2-one) and isomesityl oxide (4-methylpent-4-en-2-one) are the C_6 products; the C_9 products consist of skeletal and positional isomers of symmetric (e.g., 2,6-dimethyl-hepta-2,5-dien-4-one) and unsymmetric (e.g., 4,6-dimethyl-hepta-3,5-dien-2-one) C_9 alkanones. The canonical mechanisms for aldol condensation (Scheme 1) give symmetric C_9 alkanones via the cross-condensation of acetone with C_6 enols derived from mesityl oxide (e.g., 4-methylpenta-1,3-dien-2-ol; Scheme 1A). Unsymmetric C_9 alkanones form via cross-condensation of acetone with C_6 enols derived from isomesityl oxide (e.g., 4-methylpenta-2,4-dien-2-ol; Scheme 1B) or of C_6 alkanones with acetone-derived prop-1-en-2-ol (Scheme 1C).[38]

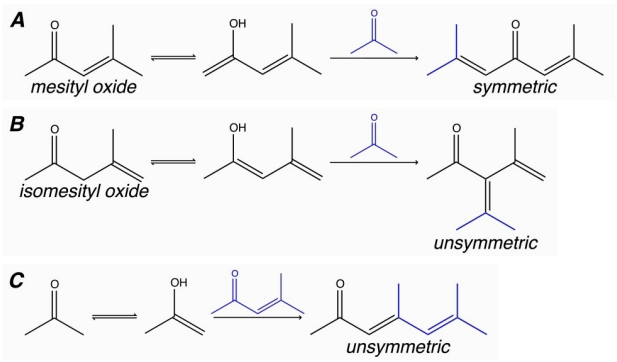

Scheme 1. Symmetric and unsymmetric C_9 alkanone products of $C_3 + C_6$ cross-condensations.

Figure 1 shows selectivities to primary C_6 alkanone products at different acetone conversions on TiO_2(a) (2.5 kPa acetone; 363 K) in the absence of intraporous *n*-heptane liquids. Acetone conversions were varied through changes in residence time or via deactivation, with identical consequences for selectivity trends; this shows that Ti–O Lewis acid-base site pairs are involved in the formation of both C_6 and C_9 alkanones. The asymptotic C_6 selectivity (extrapolated to zero conversion) is smaller than unity, indicative of the formation of both C_6 and C_9 alkanones in a single surface sojourn. The zero-conversion asymptotic ratio of unsymmetric C_9 (**B** and **C** in Scheme 1) to symmetric C_9 (**A** in Scheme 1) products is essentially zero (Figure 1) and increases monotonically as conversion increases. These data indicate that symmetric C_9 alkanones form as primary products and that secondary reactions are responsible for the formation of symmetric and unsymmetric C_9 alkanones. The self-condensation of acetone gives mesityl and isomesityl oxide and sequential reactions of bound C_6 products before desorption give *primary* C_9 alkanones. The cross-condensations of acetone and primary C_6 alkanones in subsequent surface sojourns give *secondary* C_9 alkanones. The observed relationship between product rank (primary or secondary) and C_9 alkanone (un)symmetry (Figure 1) is consistent with accepted mechanisms for aldol condensation, which involve C_3 and C_6 enols as intermediates (Scheme 1), suggesting that the elementary step sequences for the self- and cross-condensation of acetone on TiO_2(a) proceed through mechanisms akin to the accepted ones but instead with bound C_3 and C_6 enolates as intermediates.

These observations, taken together with the linear dependence of turnover rates on acetone pressure (*vide infra*), indicate that self-condensation of acetone and cross-condensation of acetone with C_6 alkanones proceed via the elementary steps depicted in Scheme 2, with prop-1-en-2-olate (C_3*) formation from acetone (C_3) reactions on bare Ti–O site pairs (*) (Step 1; Scheme 2) as the sole kinetically-relevant step in the elementary step sequences for both the self and cross-condensation reactions, as also shown previously from kinetic, isotopic, and theoretical evidence.[14,27] Acetone condensation turnover rates (per exposed Ti–O Lewis acid-base site pair) on TiO_2(a) are proportional to acetone pressure with rate constants for $(CH_3)_2CO$ and $(CD_3)_2CO$ condensation giving rise to the expected normal kinetic isotope effect.[14,27] The DFT-derived free energy barrier for C_3* formation is higher than those for subsequent C–C bond formation steps. This C_3* formation transition state (TS) gives kinetic isotope effects in agreement with measured values; it shows a significant elongation of the α-C–H bond in acetone (0.1103 nm) at the TS (0.1403 nm).[14,27]

The elementary steps after the formation of C_3* enolates complete acetone self-condensation and cross-condensation turnovers; they involve a second acetone molecule reacting with C_3* to give a TiO_2(a)-bound C_6 enolate (C_6*) (Step 2; Scheme 2), which either desorbs (Step 3) to give mesityl or isomesityl oxide (lumped as C_6 products) or reacts with another acetone molecule (Step 4) to form *primary* C_9 products (lumped as C_9' products). C_6 alkanones formed in a single surface sojourn can react with a C_3* (Step 5) to form the *secondary* C_9 products (lumped as C_9'' products). The catalytic sequences that form C_6, C_9', and C_9'' share C_3* enolate formation (Step 1) as a common

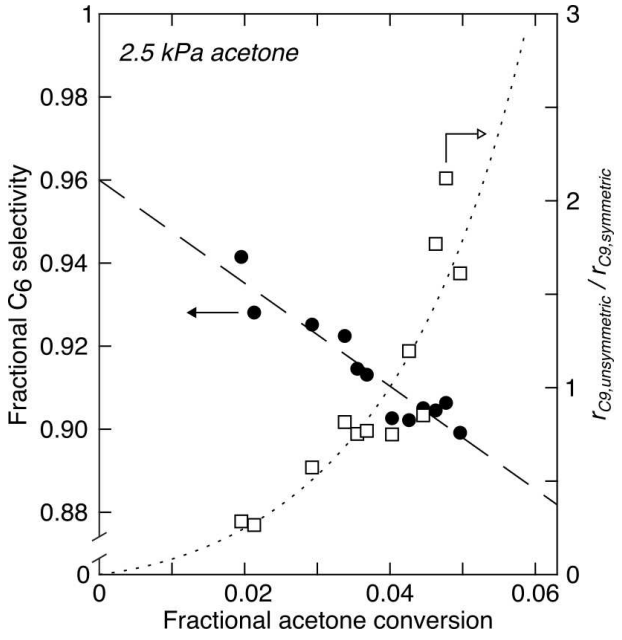

Figure 1. Fractional selectivity to C_6 alkanones (*left ordinate*, filled circles; Equation 30) and ratio of rate of unsymmetric C_9 alkanone formation to rate of symmetric C_9 alkanone formation (*right ordinate*, open squares) versus fractional conversion for acetone condensation on TiO_2(a) at 363 K and 2.5 kPa acetone. The dashed and dotted lines represent trend curves.

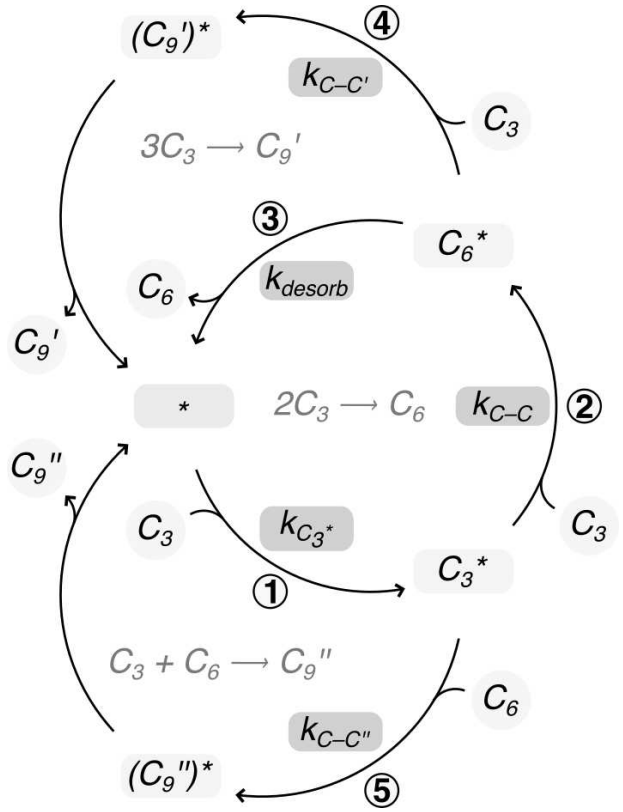

Scheme 2. Elementary steps for aldol condensation of acetone on TiO_2(a).

irreversible elementary step. Thus, the rate of the kinetically-relevant enolate formation step (Equation 1 [Eq. (1)]) is given by the combined molar rates of formation of C_6, C_9', and C_9'',

$$r_{enol} = r_1 = r_{C_6} + r_{C_9'} + r_{C_9''} \quad (1)$$

Scheme 2 and Equation 1 provide the context used in what follows to describe reactivity, selectivities, and deactivation rates for acetone condensation reactions on TiO_2(a) in the presence or absence of intrapore *n*-heptane condensation within TiO_2(a) mesopores through the formalism of transition-state theory.

Acetone condensation rates and deactivation within liquid-free TiO_2(a) mesopores

Enolate formation rates per exposed Ti–O site pair ($[Ti–O]_0$ = 3.7 nm^{-2}, measured via propanoic acid titration during acetone reactions) decreased with time-on-stream after initial contact with reactants at all acetone pressures (Figure 2). The slope of such trends (Figure 2) gives the first-order deactivation constant ($-k_d$, Equation 2 [Eq. (2)])

$$\frac{r(t)}{r(t_0)} = \exp(-k_d t) \quad (2)$$

where $r(t)$ and $r(t_0)$ denote, respectively, the rates at any time t and upon initial contact with reactants (t_0). The mean catalyst life (k_d^{-1}) decreased with increasing acetone pressure, because secondary C–C bond formation events become more prevalent and lead to the formation of larger molecules that bind strongly at Ti–O pairs.[35–36]

Enolate formation rates extrapolated to the time of initial contact with reactants reflect the properties of bare TiO_2(a) surfaces before active sites are titrated by strongly-bound products. Such initial rates are strictly proportional to acetone pressure (Figure 3), consistent with the sole kinetic relevance of prop-1-en-2-olate formation elementary steps (Step 1; Scheme 2) and with unoccupied Ti–O site pairs as the most abundant surface species; enolate formation rates are then given by Equation 3 [Eq. (3)]:

$$\frac{r_{enol(g)}}{[Ti-O]_0} = k_{C_3^*(g)} P_{acetone} \quad (3)$$

with $[Ti–O]_0$ as the total concentration of exposed Ti–O site pairs (3.7 nm^{-2}). This first-order rate constant, $k_{C_3^*(g)}$ (*"(g)"* denotes their value at conditions leading to gas-filled TiO_2(a) pores in contrast to liquid-filled pores; *vide infra*), reflects the free energy of the prop-1-en-2-olate (C_3*) formation TS referenced to those of a bare Ti–O site pair and gaseous acetone reactants.

The stability of bound molecular species and transition states species depends on outer sphere environments beyond the point of binding, as in the case of voids of molecular dimensions[37] or a liquid phase;[29,30] such interactions comple-

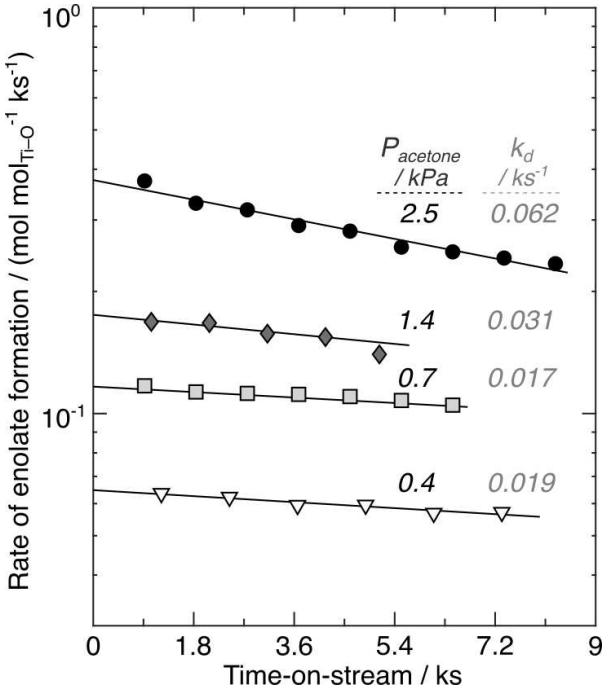

Figure 2. Rates of enolate formation per exposed Ti–O site pair (3.7 nm^{-2}) versus time-on-stream for acetone condensation on TiO_2(a) at 363 K and 0.4 kPa (▼), 0.7 kPa (■), 1.4 kPa (♦), and 2.5 kPa (●) acetone. The solid lines are lines of best fit obtained upon regression of data to Equation 2.

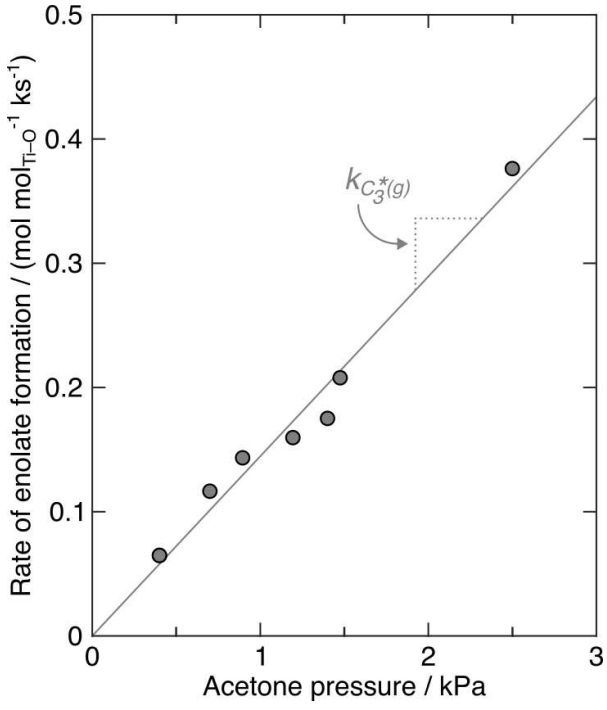

Figure 3. Rates of enolate formation per exposed Ti–O site pair (3.7 nm^{-2}) extrapolated to the time of initial contact of acetone reactants versus acetone pressure on TiO_2(a) at 363 K. The solid line is the line of best fit obtained upon linear regression of data to Equation 3; the slope, $k_{C_3^*(g)}$ = 0.14 (kPa Ti–O ks)$^{-1}$, is the first-order rate constant.

ment those conferred upon such species by direct binding at catalyst surfaces.[29–31,37] The consequences of such interactions for reactivity are most evident when kinetically-relevant steps involve adsorption (entry) or desorption (exit) steps, because the bonds with the surface are incomplete at their respective transition states. These entry and exit steps are invariably exothermic and endothermic, respectively, leading to TS structures that occur either early or late along the reaction coordinate, thus exhibiting significant reactant or product character[31–32] because they reside, in part, within the outer sphere environment; as a result, they sense outer sphere solvation effects by inorganic or organic moieties located beyond the binding point.

These outer sphere solvation effects are evident in previous work from the contrasting effects of liquids on rates of methylcyclohexene hydrogenation on Pt and Pd catalysts.[31–32,44-45] Rates of methylcyclohexene hydrogenation on Pt are higher when a liquid is present because they reflect the rate of an entry step: the (dissociative) adsorption of H_2. The outer sphere environment stabilizes the early TS for this entry step, thus increasing turnover rates on Pt. In contrast, neither the presence nor the identity of the liquid solvent influences rates of methylcyclohexene hydrogenation on Pd because the kinetically-relevant step occurs neither early nor late along its reaction coordinate; it involves a bimolecular surface reaction between two Pd-bound intermediates. The TS for this step is predominantly stabilized by direct binding at the Pd surface: the inner sphere environment.

In the case of acetone condensation, the kinetically-relevant enolate formation is an entry step (Step 1; Scheme 2) and the desorption of the bound C_6 enolates formed as primary products (Step 3) allows the "exit" of such species before subsequent C–C bond formation steps, which form C_9 alkanones (Step 4) and deactivating residues in a single surface sojourn. Thus, rates of enolate formation, primary selectivities, and deactivation constants are expected to sense the presence of a surrounding liquid phase that can interact with the relevant entry and exit transition states. *n*-Heptane is used here as the liquid because of its inert character, high mutual solubility with acetone, and a vapor pressure at 300–400 K (7–218 kPa) that allows intrapore condensation at modest prevalent *n*-heptane pressures.

Extent of intrapore *n*-heptane condensation within TiO_2(a) voids

TiO_2(a) voids consist of interstices of non-uniform cross-section formed by the packing of non-porous TiO_2(a) crystallites; these voids fill with a liquid phase at pressures below the saturation point of a contacting gas phase through capillary effects. The fraction of the pore volume that becomes liquid-filled can be accurately assessed using Barrett-Joyner-Halenda (BJH) treatments,[33] the accepted construct to describe multilayer formation and capillary condensation within nanometer-sized voids. The extent of pore filling depends on temperature, the pressure of the contacting gas, the molecular properties of the fluid, and the size of the voids. This fraction, or more precisely, in this case, the extent to which the active surface area becomes immersed within a liquid, determines the concomitant effects on rates, selectivities, and deactivation in acetone condensation on TiO_2(a). Here, N_2 uptakes at its normal boiling point (Figure S1a; Supporting Information (SI)) are used to determine the pore size distribution of TiO_2(a) (Figure S1b); this distribution is then used to estimate the fraction of surface area immersed within *n*-heptane liquids at each *n*-heptane pressure at reaction temperatures.

The shape of the measured N_2 isotherm at 77 K (Figure S1a) reflects the sequential formation of adsorbed layers and a bulk intrapore liquid phase as the relative pressure increases to its saturation point ($P/P_{sat} \geq 1$).[29] BJH formalisms enable deconvolution of uptakes to distinguish between guest molecules involved in multilayer adsorption and those involved in capillary condensation, thus enabling, in turn, the determination of the distribution of (cylindrical) pore sizes (Figure S1b).[33] The void size distribution can then be used to calculate equilibrium uptakes of any molecule at any temperature and pressure provided that the molecular properties of the fluid are known; the fidelity of this calculation relies on the adsorbate conforming to Langmuir idealizations, as expected here for the uptake of inert, non-polar *n*-heptane on TiO_2(a) at 363 K.

The calculated *n*-heptane uptakes at 363 K (Figure 4; filled symbols) together with the pore size distribution of TiO_2(a) (Figure S1b) can be used to estimate, through geometric

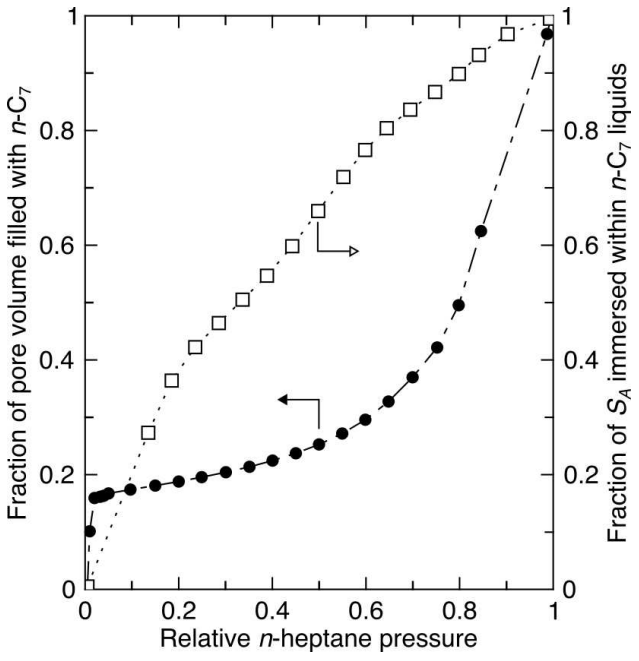

Figure 4. Calculated *n*-heptane (*n*-C_7) uptakes on TiO_2(a) (175 $m^2 g^{-1}$) versus relative *n*-heptane pressure (P/P_{sat}) at 363 K. These *n*-C_7 uptakes were calculated from measured N_2 uptakes at 77 K (Figure S1a), the BJH pore size distribution of TiO_2(a) (Figure S1b), and *n*-heptane properties (molar volume of 1.54×10^{-4} m^3 mol^{-1} and surface tension of 0.0134 J m^{-2}). The filled circles show uptakes as a fraction of the total pore volume occupied by *n*-heptane fluids on the *left* ordinate, and the open squares show uptakes as a fraction of total surface area immersed within *n*-heptane liquids on the *right* ordinate. The dash-dotted and dotted lines are guides for the eye.

arguments based on cylindrical capillary models,[29,30,33] the fraction of the TiO_2(a) surface area immersed within *n*-heptane liquids at each relative *n*-heptane pressure; Figure 4 (open symbols) shows how this fraction increases as the relative *n*-heptane pressure increases and the interstices form a liquid phase. In the next sections, the consequences of increased contact between the active TiO_2(a) surface and the intraporous non-polar liquid phase on rates, selectivities, and deactivation for acetone condensation reactions are described and interpreted to show how a solvating outer sphere environment preferentially stabilizes transition states that occur either "early" or "late" along their respective reaction coordinates.

Effects of intrapore *n*-heptane liquids on acetone condensation rates and deactivation

Figure 5 shows deactivation constants (k_d, Eq. 2) determined from regression of rate versus time data to the functional form of Equation 2 [Eq. (2)] (details in Section S2; SI) for acetone condensation reactions in the absence ($(P/P_{sat})_{n\text{-}C_7} = 0$) – and presence ($(P/P_{sat})_{n\text{-}C_7} > 0.1$) of intrapore *n*-heptane liquids; acetone and its C_6 and C_9 condensation products cannot condense to any measurable extent within the anatase pores at the conditions of this study (363 K, 0–3 kPa acetone, < 0.06 fractional acetone conversion) since the prevailing relative pressures are all smaller than 0.01. These k_d values monotonically decreased as *n*-heptane liquids increasingly filled TiO_2(a) voids (Figure 5). The mean catalyst life (k_d^{-1}) exceeds 120 ks when ~0.6 of the TiO_2(a) surfaces reside within liquid-filled voids. Such stable aldol condensation rates were previously attained only through bifunctional strategies using H_2 co-reactants to scavenge unsaturated products on a physically-mixed Cu-based hydrogenation function.[14,27] Intrapore non-polar liquids inhibit secondary C–C bond formation events and subsequent chain growth, not through chemical reactions that saturate C=O bonds in products (and reactants), but by stabilizing the TS for desorption of primary products (Step 3; Scheme 2) preferentially over those that form C–C bonds (as shown below in the context of selectivity). Such preferential stabilization of the late desorption TS that mediates an exit step is reminiscent of the effects of intrapore liquids on deactivation and selectivity for alkene dimerization on Ni-exchanged aluminosilicates.[29,30]

Enolate formation rates remained strictly proportional to acetone pressure as TiO_2(a) voids filled with liquid *n*-heptane (Figure 6), consistent with the mechanistic conclusions for reactions in gas-filled voids (*vide supra*); the sole kinetically-relevant step is still the cleavage of an α-C–H bond within acetone for C_3* formation (Step 1; Scheme 2) and the most abundant surface intermediates are still vacant Ti–O site pairs. Enolate formation rates in the presence of intrapore *n*-heptane liquids are then given by Equation 4 [Eq. (4)]:

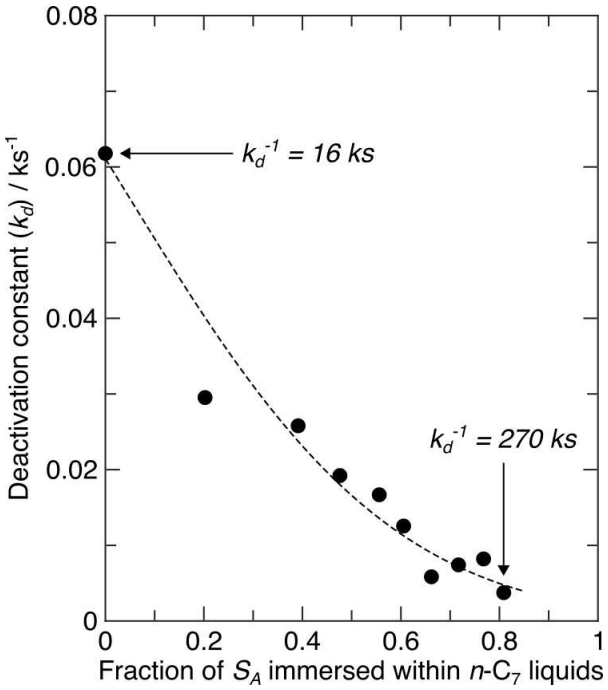

Figure 5. Deactivation constants (Eq. 2) versus fraction of TiO_2(a) surface area immersed within intrapore *n*-heptane liquids (Figure 4) for acetone condensation on TiO_2(a) at 363 K, 2.5 kPa acetone, and 0–0.63 relative *n*-heptane pressure (P/P_{sat}). The dashed line is a guide for the eye.

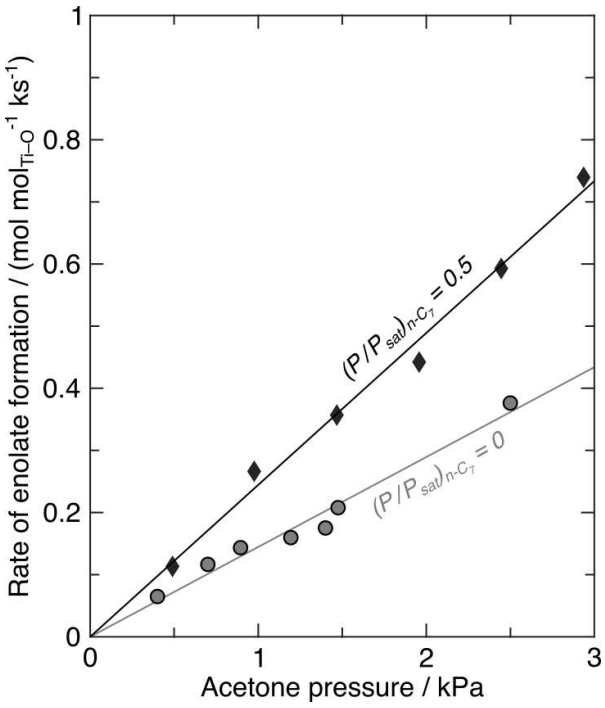

Figure 6. Rates of enolate formation per exposed Ti–O site pair (3.7 nm^{-2}) for acetone reactions on TiO_2(a) at 363 K in the absence (gray circles, $(P/P_{sat})_{n\text{-}C_7} = 0$) and presence (black diamonds, $(P/P_{sat})_{n\text{-}C_7} = 0.5$) of intrapore liquid *n*-heptane; relative *n*-heptane pressure of 0.5 corresponds to 66% of the total TiO_2(a) surface area immersed within liquid *n*-heptane (Figure 4). The gray and black solid lines are the lines of best fit obtained upon linear regression of data to Equations 3 and 4, respectively.

$$\frac{r_{enol(\ell)}}{[Ti-O]_0} = k_{C_3^*(\ell)} P_{acetone} \quad (4)$$

First-order rate constants for C_3* formation ($k_{C_3^*(\ell)}$; "(ℓ)" denotes liquid-filled TiO_2(a) pores) increased monotonically as voids filled with liquid with increasing *n*-heptane pressure. The data in Figure 7 (filled symbols, left ordinate) show the ratio of first-order rate constants for acetone condensation in the presence and absence of intrapore *n*-heptane liquids (χ) (Equation 5 [Eq. (5)]):

$$\chi = \frac{k_{C_3^*(\ell)}}{k_{C_3^*(g)}} \quad (5)$$

The tenets of transition state theory invoke a quasi-equilibrium between an activated complex and the reactants in an elementary step, thus requiring that the sum of chemical potentials (μ_i) for each species *i* times their stoichiometric coefficients (ν_i) be zero. The kinetically-relevant step (Step 1; Scheme 2) in acetone condensation within liquid-filled TiO_2 voids involves the reaction of dissolved acetone ($C_3(\ell)$) at a Ti–O site pair on TiO_2(a) surfaces in contact with liquid *n*-heptane ($*(\ell)$) to form a bound prop-1-en-2-olate also in contact with the liquid ($C_3*(\ell)$) (Equation 6 [Eq. (6)]),

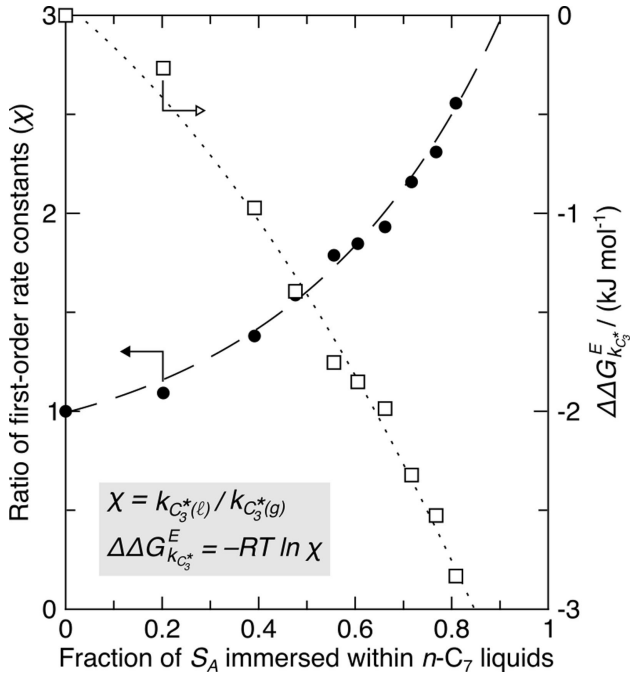

Figure 7. Ratio of rate constant for enolate formation in the presence of intrapore *n*-heptane liquids versus that in the absence of intrapore *n*-heptane liquids (*left* ordinate, filled circles; χ, Eq. 5) and excess free energy of solvation of enolate formation transition state (*right* ordinate, open squares; $\Delta\Delta G^E_{k_{C_3^*}}$, Eq. 17) versus fraction of TiO_2(a) surface area immersed within intrapore *n*-heptane liquids (Figure 4) for acetone condensation on TiO_2(a) at 363 K and 0–0.63 relative *n*-heptane pressure. The dashed and dotted lines represent trends.

$$C_3(\ell) + *(\ell) \rightleftharpoons TS_{enol}(\ell) \longrightarrow C_3*(\ell) \quad (6)$$

where $TS_{enol}(\ell)$ represents the TS for the formation of the C_3* enolate within liquid-filled voids. The equilibrated nature of the TS dictates that (Equation 7 [Eq. (7)]):

$$\mu_{TS_{enol}(\ell)} - \mu_{C_3(\ell)} - \mu*_{(\ell)} = 0 \quad (7)$$

For liquid-filled voids. In the absence of liquids, the kinetically-relevant step is (Equation 8 [Eq. (8)]):

$$C_3(g) + *(g) \rightleftharpoons TS_{enol}(g) \longrightarrow C_3*(g) \quad (8)$$

where $C_3(g)$ represents acetone in the gas phase and $*(g)$, $C_3*(g)$, and $TS_{enol}(g)$ are the bare Ti–O site pair, bound prop-1-en-2-olate, and TS for C_3* formation, respectively, within TiO_2(a) voids without a liquid phase, thus requiring that (Equation 9 [Eq. (9)]):

$$\mu_{TS_{enol}(g)} - \mu_{C_3(g)} - \mu*_{(g)} = 0 \quad (9)$$

Equations 7 and 9 can be combined with that for vapor-liquid equilibrium between the extrapore gas phase and the intrapore liquids (Equation 10 [Eq. (10)]):

$$C_3(g) \rightleftharpoons C_3(\ell) \quad (10)$$

and the consequent equality of their chemical potentials (Equation 11 [Eq. (11)])

$$\mu_{C_3(\ell)} = \mu_{C_3(g)} \quad (11)$$

to give (Equation 12 [Eq. (12)])

$$\left(\mu_{TS_{enol}(\ell)} - \mu_{TS_{enol}(g)}\right) - \left(\mu_{*(\ell)} - \mu_{*(g)}\right) = 0 \quad (12)$$

The rate of an elementary step is proportional to the number of transition states. Consequently, the ratio of enolate formation rates with ($r_{enol(\ell)}$, Eq. 4) and without ($r_{enol(g)}$, Eq. 3) the presence of a liquid (Equation 13 [Eq. (13)]):

$$\frac{r_{enol(\ell)}}{r_{enol(g)}} = \frac{[\,TS_{enol}(\ell)\,]}{[\,TS_{enol}(g)\,]} = \chi \quad (13)$$

equals the ratio of first-order rate constants for enolate formation, defined as χ in Equation 5. Equation 13 can be expressed in terms of free energy differences between transition states (TS_{enol}) and bare Ti–O site pairs (*) by:

(i) expressing the chemical potential of each species *i* in Equation 12 as [Eq. (14)]

$$\mu_i = \mu_i^\circ + RT \ln \frac{a_i}{a_i^\circ} \quad (14)$$

where a_i is the activity of species i and a_i° and μ_i° are the activity and the chemical potential of species i at some specified standard state;

(ii) choosing identical standard states for $TS_{enol}(\ell)$ and $TS_{enol}(g)$ and identical standard states for *(ℓ) and *(g) such that the a_i° and μ_i° terms for TS_{enol} and * cancel upon incorporating Equation 14 into Equation 12;

(iii) denoting a_i as the product of an activity coefficient (γ_i) and a concentration ([i]) [Eq. (15)]

$$a_i = \gamma_i [\, i \,] \quad (15)$$

and

(iv) taking bare Ti–O site pairs as the most abundant surface intermediates, as shown by the forms of the rate equations with (Eq. 4) and without (Eq. 3) intrapore liquids, such that [Eq. (16)]

$$[\, ^*(\ell) \,] = [\, ^*(g) \,] = [Ti - O]_0 \quad (16)$$

Equations 12–16 then lead to an expression for χ [Eq. (17)]

$$\chi = \exp\left(-\frac{\Delta\Delta G^E_{kc_3^*}}{RT}\right) \quad (17)$$

in terms of $\Delta\Delta G^E_{kc_3^*}$, which represents a difference in excess Gibbs free energies, defined for a given species i ($\bar{G}_i^E$) as (Equation 18 [Eq. (18)])

$$\bar{G}_i^E = RT \ln \gamma_i \quad (18)$$

$\Delta\Delta G^E_{kc_3^*}$ values reflect the difference in $\bar{G}_i^E$ values for C_3* formation transition states with and without a liquid phase ($\bar{G}^E_{TS_{enol}(\ell)} - \bar{G}^E_{TS_{enol}(g)}$) and that for Ti–O site pairs with and without a liquid phase ($\bar{G}^E_{*(\ell)} - \bar{G}^E_{*(g)}$) (Equation 19 [Eq. (19)]),

$$\Delta\Delta G^E_{kc_3^*} = \left(\bar{G}^E_{TS_{enol}(\ell)} - \bar{G}^E_{TS_{enol}(g)}\right) - \left(\bar{G}^E_{*(\ell)} - \bar{G}^E_{*(g)}\right) \quad (19)$$

These χ values increase and $\Delta\Delta G^E_{kc_3^*}$ becomes more negative as TiO_2(a) voids become increasingly filled with liquid with increasing *n*-heptane pressure (Figure 7). These trends indicate that a non-polar liquid stabilizes the C_3* formation TS to a greater extent than it stabilizes an unoccupied Ti–O site pair and that a greater fraction of the TiO_2 surface benefits from such solvation effects as liquids increasingly fill its void space.

These outer sphere solvation effects influence rates because an entry step (Step 1; Scheme 2) limits aldol condensation rates. This step involves a TS that retains some reactant-like character as it forms along the reaction coordinate; thus, it is able to sense the presence and nature of the contacting fluid phase. These significant effects of non-polar intrapore liquids on acetone condensation turnover rates on TiO_2(a) stand in contrast with the much weaker effects for ethene, propene, and butene dimerization rates observed on Ni-exchanged MCM-41, in reactions that are limited by kinetically-relevant C–C bond formation steps.[29,30] These C–C coupling steps involve bound reactants, transition states, and products that are predominantly stabilized by direct interactions with $(Ni–OH)^+$ active sites and to a lesser extent by the contacting fluid phase. In the case of acetone condensation on TiO_2(a), the C–C bond formation steps (Steps 2, 4, and 5) that occur after the kinetically-relevant entry step (Step 1) are also expected to be influenced less strongly by the nature of the outer sphere environment because, as in the case of C–C coupling on Ni-MCM-41, such steps involve bound species as reactants (C_3* in Steps 2 and 5 or C_6* in Step 4) and products (C_6*, (C_9')*, and (C_9'')* in Steps 2, 4, and 5, respectively). The transition states involved in these C–C bond formation steps do not exhibit significant reactant or product character, especially in comparison with those for entry (enolate formation) or exit (product desorption) steps that occur early or late along their respective reaction coordinates.

The bound alkene dimers formed upon kinetically-relevant C–C coupling steps on Ni-MCM-41 desorb in endothermic steps through late product-like transition states; such TS structures detect the nature of the contacting phase that accepts such species upon desorption, thus allowing them to sense the solvating properties of the intrapore phase. Consequently, the presence of a liquid makes the desorption of bound dimers favored over their sequential C–C coupling reactions, thus favoring the desorption of the initial product formed before additional C–C coupling events that lead to strongly-bound larger alkene oligomers. Consistent with such interpretations, intrapore liquids favor higher dimer selectivities and suppress deactivation to nearly undetectable extents. Similar effects of an intrapore non-polar liquid phase (*n*-heptane) on selectivity are observed here for acetone condensation on TiO_2(a) together with slower deactivation (Figure 5). These trends also reflect a preferential enhancement of desorption rates of primary C_6* enolate products (Step 3; Scheme 2) over those of subsequent C–C bond formation events during the initial reactive surface sojourn. These effects of outer sphere environments on the relative rates of exit steps and C–C bond formation events also influence selectivities to primary dimers in acetone condensation at Lewis acid-base pairs on TiO_2(a), as shown in the next section.

Effects of intrapore *n*-heptane liquids on acetone condensation selectivities

This section examines the effects of intrapore *n*-heptane liquids on selectivity and deactivation rates in the context of the stability of transition states for desorption and subsequent reactions of bound C_6 products.

Figure 8 shows the selectivity to C_6 products (S_{C_6}, Eq. 30) at different levels of acetone conversion (X), varied by changes in

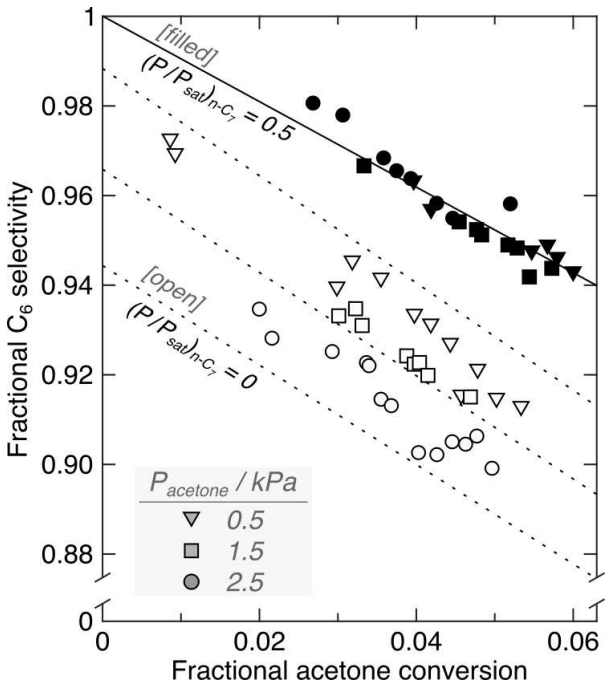

Figure 8. Fractional selectivity to C_6 alkanones (Eq. 30) versus fractional acetone conversion for acetone condensation on TiO_2(a) at 363 K; 0.5 kPa (▼), 1.5 kPa (■), and 2.5 kPa (●) acetone; and in the absence (open symbols, $(P/P_{sat})_{n\text{-}C_7} = 0$) and presence (filled symbols, $(P/P_{sat})_{n\text{-}C_7} = 0.5$) of intrapore *n*-heptane liquids. A relative *n*-heptane pressure of 0.5 at 363 K corresponds to 66% of the total TiO_2(a) surface area immersed within liquid *n*-heptane (Figure 4). The dashed and solid lines are lines of best fit obtained upon regression of data collected in the absence and presence, respectively, of intrapore *n*-heptane liquids to Equation 20.

residence time or extent of deactivation, with ($(P/P_{sat})_{n\text{-}C_7} = 0.5$; filled symbols) and without ($(P/P_{sat})_{n\text{-}C_7} = 0$; open symbols) intrapore liquids on TiO_2(a) at 0.5 kPa (triangles), 1.5 kPa (squares), and 2.5 kPa acetone (circles). C_6 selectivities extrapolated to zero conversion reflect the extent to which C_6 enolates formed in a primary C–C coupling event desorb before forming C_9 and larger chains. These asymptotic selectivities are less than one without intrapore liquids and decrease with increasing acetone pressure, indicative of rates of C_6* reactions with acetone (to form C_9'; Step 4; Scheme 2) that increase relative to those of C_6* desorption (Step 3) as acetone pressures increase. The presence of intrapore liquids leads to asymptotic C_6 selectivities near unity at all acetone pressures, consistent with a preferential increase in C_6* desorption rates (Step 3) over C–C coupling events (Step 4). Such an exit step involves a late product-like TS that is stabilized by outer sphere solvation more effectively than for subsequent C_6* reactions that involve reactants, transition states, and products that are stabilized preferentially by interactions with Lewis acid-base pairs.

C_6 selectivities decreased with increasing conversion (Figure 8) in all cases, because C_6 products readsorb at acid-base pairs along the catalyst bed and undergo subsequent C–H activation events that form C_6* enolates (and C–C coupling via reaction with acetone; Step 4; Scheme 2) or react as the electrophile in C–C coupling with bound C_3* enolates (Step 5) to form C_9'' molecules. C_6 selectivities were lower at higher acetone pressures for all conversions (Figure 8; open symbols). These trends reflect higher rates of C–C bond formation events and the prevalence of longer chains as reactants in such events as acetone pressures and conversions increase. The slopes of these selectivity-conversion trends (S_{C_6}; Figure 8) reflect the extent to which C_3 enolates, formed in the sole kinetically-relevant step, are consumed by acetone (Step 2) to ultimately form primary products (C_6 and C_9') versus the extent to which they are consumed by C_6 alkanones (Step 5) to ultimately form secondary products (C_9'').

The rate constants for Steps 2–5 (Scheme 2) account for the slope and intercept of the selectivities ($S_{C_6}(X)$) in Figure 8 in a manner that becomes evident from plug-flow reactor descriptions of the rates of primary and secondary events along the bed. The resulting coupled differential equations account for the rates of C_6, C_9', and C_9'' formation and include rate equations derived from the elementary steps in Scheme 2 (details in Section S3.1–3.3; SI).

The linear trends of C_6 selectivities (S_{C_6}) with acetone conversion (X) (Figure 8) are consistent with the predictions of these analysis protocols when only terms linear in X are retained (Equation 20 [Eq. (20)]):

$$S_{C_6}(X) = \frac{1}{1+\frac{3}{2}\Omega}\left(1 - \frac{3}{2}\Phi\left(\frac{1+\Omega}{2+3\,\Omega}\right)^2 X\right) \quad (20)$$

The Ω and Φ terms in Equation 20 represent dimensionless groups that combine kinetic parameters for Steps 2–5 in Scheme 2 [Eq. (21) and (22)],

$$\Omega = \tilde{\Omega}\, P_{acetone} = \frac{k_{C-C'} P_{acetone}}{k_{desorb}} \quad (21)$$

$$\Phi = \frac{k_{C-C''}}{k_{C-C}} \quad (22)$$

These equations are derived using an asymptotic treatment of the net rates of C_6 formation and C_3 consumption (details in Section S3.4; SI). Equation 20 accurately describes such systems when the magnitude of the ratio of the quadratic term to (X^2) to the linear term (X) in the asymptotic expansion is much smaller than unity. This ratio (which is directly proportional to both X and Φ; details in Section S3.5; SI) is calculated to be between 0.02 and 0.2 when using the best-fit $\tilde{\Omega}$ and Φ values obtained upon regression of data in Figure 8 to the functional form of Equation 20 (Table 1). These small values for estimates of the absolute relative errors combined with the absence of any systematic deviation from linearity in the S_{C_6} versus X

Table 1. Best fit $\tilde{\Omega}$ (Eq. 21) and Φ (Eq. 22) values and 95% confidence intervals obtained upon regression of C_6 selectivity versus conversion data (Figure 8) to the functional form Equation 20.

$(P/P_{sat})_{n\text{-}C_7}$	$\tilde{\Omega}$ [kPa^{-1}]	Φ
0	$(1.5 \pm 0.2)\cdot 10^{-2}$	3.3 ± 1.1
0.5	$(3.5 \pm 0.8)\cdot 10^{-5}$	2.6 ± 0.4

trends (Figure 8) show that the asymptotic linear expansion in Equation 20 is appropriate to accurately describe the data.

The Ω term accounts for the asymptotic C_6 selectivity ($X \to 0$) and is equal to the ratio of the rate of C_6* enolates reacting with acetone molecules to ultimately form C_9' (Step 4; Scheme 2) and desorbing to form C_6 (Step 3); the $\tilde{\Omega}$ term in Equation 21 is the ratio of the respective rate constants: $k_{C-C'}$ (Step 4) and k_{desorb} (Step 3). The Φ term accounts for the selectivity to secondary C_9'' products; it contains kinetic parameters for reactions of C_3* enolates derived from acetone with previously desorbed C_6 alkanones to form C_9'' products ($k_{C-C''}$, Step 5) or with acetone to form C_6* species (k_{C-C}, Step 2) that ultimately desorb as C_6 or C_9' primary products.

The solid and dashed lines in Figure 8 are derived from a regression of the selectivity data with or without intrapore liquids, respectively, to the form Equation 20, and the corresponding values of $\tilde{\Omega}$ and Φ are shown in Table 1. The $\tilde{\Omega}$ value is $(3.5 \pm 0.8) \cdot 10^{-5}$ kPa^{-1} when intrapore liquids are present ($P/P_{sat})_{n\text{-}C_7} = 0.5$); this small $\tilde{\Omega}$ value renders the denominator of the intercept in Equation 20 approximately equal to unity, consistent with asymptotic C_6 selectivities near unity (Figure 8). In contrast, the $\tilde{\Omega}$ value is much larger ($(1.5 \pm 0.2) \cdot 10^{-2}$ kPa^{-1}) in the absence of a liquid phase, consistent with the formation of C_9' primary products during initial surface sojourns in gas-filled TiO_2(a) pores. The Φ values, unlike the disparate $\tilde{\Omega}$ values, are similar for reactions with (2.6 ± 0.4) and without (3.3 ± 1.1) intrapore *n*-heptane liquids, suggesting that the outer sphere environment affects similarly the transition states mediating the initial C–C bond formation steps in both the self-condensation of acetone (Step 2; Scheme 2) and the cross-condensation of acetone with C_6 alkanones (Step 5).

As for C_3* formation rate constants (*vide supra*), transition state formalisms can be used to interpret the effects of a liquid phase on $\tilde{\Omega}$ and Φ in terms of the extent to which the relevant transition states are able to sense such outer sphere environments as a result of "lateness".

The Ω term is equal to the ratio of the rate of the elementary step for C_6* consumption by acetone ($r_{C-C'}$, Step 4; Scheme 2) to that by desorption (r_{des}, Step 3) which, in turn, corresponds to the ratio of concentrations of the respective transition states (Equation 23 [Eq. (23)]):

$$\Omega = \frac{r_{C-C'}}{r_{des}} = \frac{[\ TS_{C-C'}\ ]}{[\ TS_{des}\ ]} \tag{23}$$

where $TS_{C-C'}$ and TS_{des} are the transition states for Steps 4 and 3 (Scheme 2), respectively. The ratio of Ω values for reactions with and without *n*-heptane liquids is then given by (Equation 24 [Eq. (24)]):

$$\frac{\Omega_{(\ell)}}{\Omega_{(g)}} = \frac{[\ TS_{C-C'}(\ell)\ ]\ /\ [\ TS_{C-C'}(g)\ ]}{[\ TS_{des}(\ell)\ ]\ /\ [\ TS_{des}(g)\ ]} \tag{24}$$

This ratio depends on differences in excess Gibbs free energies ($\Delta\Delta G^E_\Omega$) (Equation 25 [Eq. (25)]):

$$\frac{\Omega_{(\ell)}}{\Omega_{(g)}} = \exp\left(-\frac{\Delta\Delta G^E_\Omega}{RT}\right) \tag{25}$$

for the formation of transition states for C–C coupling to form C_9' (Step 4) ($\bar{G}^E_{TS_{C-C'}(\ell)} - \bar{G}^E_{TS_{C-C'}(g)}$) and C_6* desorption to form C_6 (Step 3) ($\bar{G}^E_{TS_{des}(\ell)} - \bar{G}^E_{TS_{des}(g)}$) (Equation 26 [Eq. (26)]),

$$\Delta\Delta G^E_\Omega = \left(\bar{G}^E_{TS_{C-C'}(\ell)} - \bar{G}^E_{TS_{C-C'}(g)}\right) - \left(\bar{G}^E_{TS_{des}(\ell)} - \bar{G}^E_{TS_{des}(g)}\right) \tag{26}$$

The best-fit $\tilde{\Omega}$ values in Table 1 show that $\Omega_{(\ell)}/\Omega_{(g)}$ is much smaller than unity ($(2.3 \pm 0.6) \cdot 10^{-3}$) for *n*-heptane pressures leading to ~70% of the TiO_2(a) surfaces immersed within *n*-heptane liquids; this corresponds to a $\Delta\Delta G^E_\Omega$ value of $+(18 \pm 5)$ kJ mol^{-1}.

The estimated value of $\Delta\Delta G^E_\Omega$ being positive indicates that non-polar *n*-heptane liquids preferentially stabilize the TS for C_6* desorption (TS_{des}; Step 3; Scheme 2) to a much greater extent than that for C_6*-acetone C–C coupling reactions ($TS_{C-C'}$; Step 4). This reflects, in turn, a desorption TS that occurs late along the endothermic reaction coordinate and senses the outer sphere environment to a greater extent than the TS for the reaction between a bound C_6* and acetone, which is preferentially stabilized by coordination at Ti–O site pairs. These preferential solvation effects on selectivity also underpin the observed effects in intrapore liquids on deactivation rates (Figure 5) by enhancing desorption rates not only of C_6* species but also of larger oligomers, thus inhibiting their further growth.

The rates of C_3* reactions with C_6 alkanones to form C_9'' ($r_{C-C''}$, Step 5; Scheme 2) and with acetone to form C_6 or C_9' (r_{C-C}, Step 2) give an expression analogous to Equation 25 but for the parameter Φ (Equation 27 [Eq. (27)]):

$$\frac{\Phi_{(\ell)}}{\Phi_{(g)}} = \exp\left(-\frac{\Delta\Delta G^E_\Phi}{RT}\right) \tag{27}$$

where $\Delta\Delta G^E_\Phi$ is the difference in excess Gibbs free energies for the formation of the TS for Step 5 ($\bar{G}^E_{TS_{C-C''}(\ell)} - \bar{G}^E_{TS_{C-C''}(g)}$) and Step 2 ($\bar{G}^E_{TS_{C-C}(\ell)} - \bar{G}^E_{TS_{C-C}(g)}$) (Equation 28 [Eq. (28)]):

$$\Delta\Delta G^E_\Phi = \left(\bar{G}^E_{TS_{C-C''}(\ell)} - \bar{G}^E_{TS_{C-C''}(g)}\right) - \left(\bar{G}^E_{TS_{C-C}(\ell)} - \bar{G}^E_{TS_{C-C}(g)}\right) \tag{28}$$

The best-fit Φ values in Table 1 show that $\Phi_{(\ell)}/\Phi_{(g)}$ is near unity ($(7.9 \pm 2.9) \cdot 10^{-1}$) when ~70% of the total TiO_2(a) surface area is immersed within *n*-heptane liquids, corresponding to a $\Delta\Delta G^E_\Phi$ value near zero ((0.72 ± 0.21) kJ mol^{-1}). Thus, the intrapore *n*-heptane liquid phase affords similar stabilization to both of the transition states mediating C–C coupling with bound prop-1-en-2-olates. These transition states likely involve strong covalent interactions between organic moieties and isolated Ti–O site pairs and only weak long-range interactions with the

outer sphere environment because such solvation effects would otherwise preferentially stabilize the larger C_3*–C_6 coupling TS (Step 5) over the smaller C_3*–C_3 coupling TS (Step 2) and lead to negative $\Delta\Delta G^{E}_{\Phi}$ values.

The preferential stabilization of C_6 product desorption transition states over those for C–C coupling of bound C_6 species with acetone by *n*-heptane liquids accounts for the higher primary C_6 selectivities; it also leads to the less frequent occurrence of the rare events that form stranded larger oligomers responsible for the titration of Ti–O acid-base pairs. The stability and reactivity conferred by such a liquid phase here for acetone condensation below 400 K was achieved previously only at about ~500 K through scavenging of primary unsaturated alkanones enabled by the presence of H_2 and a physically-mixed Cu function;[14,27] at these higher temperatures, desorption becomes quasi-equilibrated, thus allowing the conversion of these initial products to less reactive ones at a remote hydrogenation function. The effects of intrapore *n*-heptane liquids on turnover rates, deactivation rates, and primary selectivities reported here for acetone condensation on TiO_2(a) share mechanistic underpinnings with those observed previously for alkene dimerization on Ni-exchanged aluminosilicates.[29,30] These solvation effects reflect, in both cases, the preferential stabilization of the late product-like transition states that mediate exit steps for primary product desorption. The reactant-like transition states involved in the entry step that forms C_3* enolates in the kinetically-relevant step for acetone condensation also senses the outer sphere environment, leading to turnover rates that benefit from the presence of a non-polar liquid as the contacting phase, a trend that was not observed in alkene dimerization because the TS for its kinetically-relevant step was preferentially stabilized by direct binding with acid-base site pairs.

The non-covalent dispersive interactions between a non-polar liquid and early or late transition states lead to higher turnover rates and primary product selectivities and to lower deactivation rates in acetone condensation reactions on TiO_2. Such enthalpic effects are reminiscent of those conferred through host-guest interactions within inorganic voids in zeotypes,[37,40] but do not impose the enthalpic penalties inherent in the inorganic void and organic TS distortions required to minimize the free energy in such catalytic systems.[41] The distortions required to benefit from outer sphere stabilization incur a much lower enthalpic penalty in the case of liquids. In addition, the diversity of chemical properties and volatility provided by liquids and their ability to condense within mesopores of different size and containing different catalytic functions significantly extend the types and sizes of TS structures and chemical reactions known to benefit from confinement within inorganic voids of molecular dimensions.[40–42]

Conclusions

n-Heptane liquids formed within the interstices between exposed anatase surfaces accelerate turnover rates, attenuate deactivation, and increase selectivity to primary products during acetone condensation on Ti–O Lewis acid-base site pairs. These solvation effects are all consequences of the preferential stabilization afforded by the dense non-polar fluid phase to the transition states that mediate entry and exit steps within the closed and open elementary step sequences for the formation of alkanone products and deactivating residues. First-order rate constants for acetone condensation reflect the free energy of formation of the transition state mediating the entry step of dissociative adsorption of a free acetone molecule onto a bare Ti–O site pair to form a bound prop-1-en-2-olate. The intraporous *n*-heptane liquids solvate this early reactant-like transition state via stabilizing van der Waals contacts between solvent molecules and the organic moieties at the transition state of this entry step, thereby accelerating rates of acetone condensation. These liquids also effect decreased deactivation rates and increased selectivities to primary C_6 products by stabilizing preferentially the late product-like transition state mediating the exit step of desorption of TiO_2-bound C_6 enolates, formed upon initial C–C bond formation between acetone and TiO_2-bound prop-1-en-2-olate, over the transition states mediating subsequent C–C bond formation steps that lead to the formation of strongly bound C_{9+} inhibitors or unselective primary C_9 alkanone products. Such protection against deactivation was achieved previously only through bifunctional strategies that terminate aldol condensation cascades by hydrogenating alkenone products on a physically mixed Cu function prior to subsequent C–C bond formation events.[14,27] The consequences of non-polar intrapore liquids shown here for acetone condensation on TiO_2 demonstrates that the versatility of this approach to affect deactivation rates and selectivity extends beyond alkene dimerization on Ni-exchanged aluminosilicates,[29,30] suggesting apposite this approach to other complex reaction networks that suffer from low rates, short catalyst lifetimes, and poor selectivity or those in which rapid deactivation hinders mechanistic inquiries.

Experimental Methods

Catalyst treatment and characterization

The anatase phase of TiO_2 (TiO_2(a)) was chosen for study because aldol condensation turnover rates are much higher than on its rutile form, a consequence of the formation of stable proton adducts on the latter that titrate Ti–O pairs.[14] TiO_2(a) powders (Alfa Aesar, 99.7%; 175 $m^2 g^{-1}$) were treated in flowing air (1.7 $cm^3 g^{-1}$ s^{-1}; Praxair, ultra zero grade) at 673 K (0.17 K s^{-1}) for 3 h. TiO_2(a) aggregates (180–250 μm) were prepared by pressing, crushing, and sieving fine TiO_2(a) powders. N_2 physisorption uptakes were measured at its normal boiling point (after evacuating samples by heating to 573 K at 0.083 K s^{-1} and holding for 3 h) using a volumetric adsorption unit (Micromeritics, ASAP 2020). The mathematical formalisms used to determine pore size distributions and *n*-heptane uptakes at 363 K from measured N_2 uptakes at 77 K are described in Results and Discussion.

Catalytic rate measurements

TiO_2(a) aggregates were held on a porous quartz disc within a tubular quartz reactor (7.0 mm i.d.) with plug-flow hydrodynamics. The reactor was placed within a three-zone resistively-heated furnace (Applied Test Systems Inc.); temperatures were controlled using electronic temperature controllers (Watlow) and measured using a K-type thermocouple (Omega) affixed to the outer wall of the quartz reactor near the axial bed midpoint. Catalysts were treated in flowing He (5.6 $cm^3 g^{-1} s^{-1}$; Praxair, 99.999%) by heating to 543 K (at 0.083 $K s^{-1}$) and holding for 3 h before cooling to reaction temperatures. Helium flow rates were metered using mass flow controllers (Porter, Inc.). Acetone (Sigma-Aldrich, $\geq$99.9%) and *n*-heptane (Sigma-Aldrich, $\geq$99%) were introduced as liquids using syringe pumps (KD Scientific) and vaporized into heated transfer lines ($\geq$403 K). The identity and concentration of reactants and products in reactor inlet and effluent streams were determined using a gas chromatograph (Agilent 6890 A) equipped with a methyl silicone column (Agilent HP-1, 50 m × 0.32 mm × 1.05 μm) and a flame ionization detector. Retention times and response factors were determined from acetone (Sigma-Aldrich, $\geq$99.9%), mesityl oxide (Spectrum Chemicals, 98%), 2,6-dimethyl-hepta-2,5-dien-4-one (Sigma-Aldrich, 95%), 4,6-dimethyl-hepta-3,5-dien-2-one (Sigma-Aldrich, 95%), and *n*-heptane (Sigma-Aldrich, $\geq$99%) standards.

Acetone reactions on TiO_2(a) at the examined conditions give isomers of alkanones with six ($C_6H_{10}O$) and nine ($C_9H_{14}O$) carbon atoms as products. The C_6 alkanone isomers are mesityl oxide (4-methylpent-3-en-2-one) and isomesityl oxide (4-methylpent-4-en-2-one), and the C_9 alkanone isomers comprise dienones with C=C double bonds at various positions along five- and seven-carbon backbones (Scheme 1). Thermodynamic data[28,34] were used to determine approach to equilibrium values ($\eta_{n,j}$) for acetone conversion to primary products, defined here as (Equation 29 [Eq. (29)]):

$$\eta_{n,j} = \frac{1}{K_{n,j}} \left(\frac{P_{C_{3n,j}} \left(P_{H_2O}\right)^{n-1}}{\left(P_{C_3}\right)^{n}} \right), \quad n = 2 \text{ or } 3 \tag{29}$$

where P_{C_3}, $P_{C_{3n,j}}$, and P_{H_2O} are the pressures of acetone, C_6 ($n = 2$) or C_9 ($n = 3$) acetone condensation products, and water, respectively (in units of bar), and $K_{n,j}$ is the equilibrium constant for acetone condensation to the j^{th} isomer of aldol condensation products with 3*n* C-atoms. These $\eta_{n,j}$ values were smaller than 10^{-2} at all conditions and for all C_6 and C_9 product isomers, indicating that measured rates accurately reflect the forward rates of each reaction.

Acetone condensation rates are reported based on the number of Ti–O Lewis acid-base site pairs, determined by titration of such pairs with propanoic acid during acetone reactions (3.7 Ti–O centers nm^{-2}[14]). Selectivities to C_6 and C_9 alkanones (S_{3n}, $n = 2$ or 3) are reported on a carbon basis (Equation 30 [Eq. (30)]):

$$S_{3n} = \frac{\sum_{j \text{ isomers}} \left(n \cdot r_{C_{3n,j}} \right)}{\sum_{n=2 \text{ or } 3} \sum_{j \text{ isomers}} \left(n \cdot r_{C_{3n,j}} \right)} \tag{30}$$

where $r_{C_{3n,j}}$ is the molar rate of formation of the j^{th} isomer of alkanone product with 3*n* C-atoms. Regressions of rate and selectivity data to Equations 2, 3, 4, and 20 (*vide supra*) were performed using known and established methods implemented either in MATLAB or Athena Visual Studio[43] codes.

Acknowledgements

This work was supported by the U.S. Department of Energy (DOE) and Office of Basic Energy Sciences under contract number DE-AC05-76RL0-1830.

Conflict of Interest

The authors declare no conflict of interest.

Data Availability Statement

The data that support the findings of this study are available from the corresponding author upon reasonable request.

Keywords: Aldol reaction · Capillary condensation · Heterogeneous catalysis · Solvent effects · Titania

[1] G. W. Huber, J. N. Chheda, C. J. Barrett, J. A. Dumesic, *Science* **2005**, *308*, 1446–1450.
[2] Y. Román-Leshkov, J. N. Chheda, J. A. Dumesic, *Science* **2006**, *312*, 1933–1937.
[3] E. L. Kunkes, D. A. Simonetti, R. M. West, J. C. Serrano-Ruiz, C. A. Gärtner, J. A. Dumesic, *Science* **2008**, *322*, 417–421.
[4] D. A. Simonetti, J. A. Dumesic, *Catal. Rev.* **2009**, *51*, 441–484.
[5] D. M. Alonso, J. Q. Bond, J. A. Dumesic, *Green Chem.* **2010**, *12*, 1493–1513.
[6] J. C. Serrano-Ruiz, R. M. West, J. A. Dumesic, *Annu. Rev. Chem. Biomol. Eng.* **2010**, *1*, 79–100.
[7] D. M. Alonso, S. G. Wettstein, J. A. Dumesic, *Chem. Soc. Rev.* **2012**, *41*, 8075–8098.
[8] S. Chu, A. Majumdar, *Nature* **2012**, *488*, 294–303.
[9] H. Idriss, K. S. Kim, M. A. Barteau, *J. Catal.* **1993**, *139*, 119–133.
[10] S. Luo, J. L. Falconer, *J. Catal.* **1999**, *185*, 393–407.
[11] J. I. Di Cosimo, G. Torres, C. R. Apesteguía, *J. Catal.* **2002**, *208*, 114–123.
[12] J. E. Rekoske, M. A. Barteau, *Ind. Eng. Chem. Res.* **2011**, *50*, 41–51.
[13] V. E. Collier, N. C. Ellebracht, G. I. Lindy, E. G. Moschetta, C. W. Jones, *ACS Catal.* **2016**, *6*, 460–468.
[14] S. Wang, K. Goulas, E. Iglesia, *J. Catal.* **2016**, *340*, 302–320.
[15] Z. D. Young, S. Hanspal, R. J. Davis, *ACS Catal.* **2016**, *6*, 3193–3202.
[16] H. Zhang, M. Y. S. Ibrahim, D. W. Flaherty, *J. Catal.* **2018**, *361*, 290–302.
[17] S. Shylesh, L. A. Bettinson, A. Aljahri, M. Head-Gordon, A. T. Bell, *ACS Catal.* **2020**, *10*, 4566–4579.
[18] K. Okumura, Y. Iwasawa, *J. Catal.* **1996**, *164*, 440–448.
[19] R. Martinez, M. C. Huff, M. A. Barteau, *J. Catal.* **2004**, *222*, 404–409.
[20] T. N. Pham, T. Sooknoi, S. P. Crossley, D. E. Resasco, *ACS Catal.* **2013**, *3*, 2456–2473.
[21] M. J. Climent, A. Corma, S. Iborra, *Green Chem.* **2014**, *16*, 516–547.
[22] G. Pacchioni, *ACS Catal.* **2014**, *4*, 2874–2888.
[23] T. N. Pham, D. Shi, D. E. Resasco, *Top. Catal.* **2014**, *57*, 706–714.
[24] S. Tosoni, G. Pacchioni, *J. Catal.* **2016**, *344*, 465–473.
[25] S. Wang, E. Iglesia, *J. Catal.* **2017**, *345*, 183–206.
[26] H. Idriss, M. A. Barteau, *Catal. Lett.* **1994**, *26*, 123–139.
[27] S. Wang, E. Iglesia, *J. Phys. Chem. C* **2016**, *120*, 21589–21616.
[28] S. Herrmann, E. Iglesia, *J. Catal.* **2018**, *360*, 66–80.
[29] I. Agirrezabal-Telleria, E. Iglesia, *J. Catal.* **2017**, *352*, 505–514.
[30] I. Agirrezabal-Telleria, E. Iglesia, *J. Catal.* **2020**, *389*, 690–705.
[31] E. E. Gonzo, M. Boudart, *J. Catal.* **1978**, *52*, 462–471.
[32] R. J. Madon, E. Iglesia, *J. Mol. Catal. A* **2000**, *163*, 189–204.
[33] E. P. Barrett, L. G. Joyner, P. P. Halenda, *J. Am. Chem. Soc.* **1951**, *73*, 373–380.
[34] J. P. Guthrie, *Can. J. Chem.* **1978**, *56*, 962–973.
[35] E. E. Wolf, E. E. Petersen, *J. Catal.* **1977**, *47*, 28–32.
[36] J. W. Lee, J. B. Butt, D. M. Downing, *AIChE J.* **1978**, *24*, 212–222.
[37] A. Bhan, E. Iglesia, *Acc. Chem. Res.* **2008**, *41*, 559–567.

[38] M. Loudon, *Organic Chemistry*, 5th ed.; Roberts and Company Publishers, 2009.
[39] D. Ruthven, *Principles of Adsorption and Adsorption Processes*; John Wiley & Sons, 1984.
[40] R. Gounder, E. Iglesia, *Chem. Commun.* **2013**, *49*, 3491–3509.
[41] M. L. Sarazen, E. Iglesia, *ChemCatChem* **2018**, *18*, 4028–4037.
[42] E. Iglesia, In *Proceedings Of The 24th International Solvay Conference*; K. Wüthrich, R. H. Grubbs, T. Visart de Bocarmé, A. De Wit, Eds.; *Catalysis in Chemistry and Biology*; World Scientific Publishing, August **2018**; pp 148–155.
[43] W. E. Stewart and M. Caracotsios, Computer-Aided Modeling of Reactive Systems; John Wiley & Sons, **2008**.
[44] R. J. Madon, J. P. O'Connell, M. Boudart, *AIChE J.* **1978**, *24*, 904–911.
[45] E. Segal, R. J. Madon, M. Boudart, *J. Catal.* **1978**, *52*, 45–49.

Manuscript received: January 14, 2022
Revised manuscript received: March 25, 2022
Version of record online: May 4, 2022